Defect-activated versus intrinsic Raman spectra of GdN and LuN

K. Van Koughnet,[1] H. J. Trodahl,[2] W. F. Holmes-Hewett,[1] and B. J. Ruck[1]
[1]*The MacDiarmid Institute for Advanced Materials and Nanotechnology, The School of Chemical and Physical Sciences, Victoria University of Wellington, PO Box 600, Wellington 6140, New Zealand*
[2]*The School of Chemical and Physical Sciences, Victoria University of Wellington, PO Box 600, Wellington 6140, New Zealand*

(Received 23 January 2023; revised 26 June 2023; accepted 27 July 2023; published 9 August 2023)

We report Raman studies of GdN and LuN, two of the rare-earth mononitrides that form a series of mostly *intrinsic* ferromagnetic semiconductors. Their rock-salt structure supports no first-order Raman scattering, but, nonetheless, we find a density-of-modes pattern expected for nearly point-defect scattering, an intrinsic two-phonon scattering spectrum, and an LO feature that appears independent of defect concentration. The results are compared with the phonon dispersion calculated within a density functional theory treatment indicating that computed phonon frequencies are smaller than measured, with the disagreement rising to ∼30% for the TA branch. Contrary to the previous assumption of defect-induced scattering at the L point, we propose that the observed LO feature arises from LO(Γ) scattering induced by the Fröhlich interaction, similar to what has been observed in YbS.

DOI: 10.1103/PhysRevB.108.064306

I. INTRODUCTION

The trivalent preference of the rare earths ensures that they react freely with the pnictides, adopting a NaCl structure. The heavier pnictides are antiferromagnetic, and in that company, the nitrides stand out for their ferromagnetic order at cryogenic temperatures [1,2]. Electronically, the LnN (Ln is a lanthanide element) are mostly narrow-gap semiconductors, marking the series as unique mutually epitaxy-compatible *intrinsic* ferromagnetic semiconductors. Their strongly ionic nature ensures Ln $5d$ conduction and N $2p$ valence bands, although complicated by intersecting Ln $4f$ bands [2]. Within that scenario it is the coupled electronic/magnetic properties that have seen attention, both theoretical and experimental, whereas, vibrational studies are rare. Notably the phonon contributions to specific heat and thermal transport are of technological importance for the use of several LnN as working materials for adiabatic-demagnetization cooling [3].

The NaCl structure of the LnN ensures an IR-active TO(Γ) mode, and the frequency of that mode has been reported for about half of the series [4]. In contrast there is no first-order Raman activity within the NaCl structure, although several groups have reported what is apparently disorder-activated Raman signals in the LnN and the closely related Eu monoxide EuO [5–9]. Attention has focused primarily on a moderately strong Raman feature in the 500–600 cm^{-1} range that we believe has been incorrectly interpreted as an LO(L) vibration activated by crystal defects [6,7,10] or spin disorder [9]. The relatively small activation energy of nitrogen vacancies renders them common within the LnN, suggesting them as likely candidates for a Raman-activating defect, although no clear nitrogen-vacancy dependence has been found [10].

Weakening of wave-vector conservation from point defects, of which N vacancies are an example, is expected to show Raman spectra that follow the density of modes (DOM), weighted by the level of participation of the specific defect in the various normal-mode vibrations and the consequent modulation of the polarizibility at the frequency of excitation laser line. Indeed our data below do show a DOM pattern, although with an anomalous enhancement of the LO feature compared to the DOM pattern for the rest of the optic branches. Similar symmetry-forbidden Raman scattering from LO modes is not unknown within rock-salt structures [11,12], and as mentioned above was noted already more than 40 yr ago in the very similar Eu monochalcogenides [9]. There is a literature seeking an understanding of that scattering [13], although to our knowledge no single model can explain all such instances.

This paper reports scattering by both an LO mode and the DOM excitations in two LnN (GdN and LuN) and compares them to DOM patterns calculated within a density functional theory (DFT) formalism. These are the two LnN in which the $4f$ states are far ($\geqslant$ 5 eV) from the band gap, so with minimum influence on phonon dispersion. There remains a strong contrast, however, as regards the spin magnetic moment carried by the $4f$ shell, zero in LuN but forming a series maximum of 7 μ_B in GdN [2]. We report also an investigation of the effects of deliberately introduced nitrogen vacancies, which indicate they are certainly not the defect rendering the LO mode Raman active. The weaker broad scattering is demonstrated as a combination of single-phonon scattering activated by defects and symmetry-allowed two-phonon scattering.

II. EXPERIMENTAL/COMPUTATIONAL DETAILS

The films used in the present paper were grown by evaporating the lanthanide in the presence of molecular nitrogen. Freshly evaporated lanthanide surfaces catalyze breaking of the N_2 triple bond, permitting growth without activation [14,15]. However, activation of the nitrogen

is required for two of the lanthanides Eu and Yb and for comparison, here, we grew a selection of the present films also in nitrogen from a Kaufmann ion source. Below, we report Raman spectroscopy on films grown to a thickness of typically 100 nm on *c*-plane sapphire. AlN passivating caps controlled the propensity of the LnN to react with oxygen. To establish the dependence of Raman signals on various defects they were grown onto substrates held at various temperatures, which acts to control the concentration V_N of nitrogen vacancies. The V_N concentration was low, on the order of a few percent or less, and the effect on their conductivity was measured and used as a proxy for their concentration as discussed in the next sections.

Ambient-temperature Raman spectroscopy was performed with a Jobin-Yvon LabRam fitted with a microscope. The resolution used was ~ 1 cm^{-1}, substantially finer than the features in LnN film spectra. The reported measurements were performed with 514-nm (2.43-eV) excitation from an Ar^+ laser. Limited measurements using 458 nm (2.71 eV) and 633 nm (1.96 eV) showed no significant spectral differences. The incident power was held below 1 mW to avoid significant heating of the samples.

In order to have vibration-frequency comparisons based on current computational platforms, DFT-based calculations were undertaken for GdN and LuN using QUANTUM ESPRESSO [16–20] and pseudopotentials from Topskal and Wentzcovitch [21]. To model the electronic structure of these materials more accurately, a Hubbard U term is typically used to push the $4f$ and $5d$ states away from the Fermi level. In the present paper, we have only applied a Hubbard U to the $5d$ states alone on GdN and LuN. As in our previous works, we have chosen the Hubbard U on the $5d$ states to reproduce the experimental optical band gap for each material [22,23]. For a fuller description of the Hubbard treatments in the LnN see earlier publications [23–25]. The DFT calculations were undertaken at the experimental lattice parameters of 4.99 and 4.785 Å for GdN and LuN, respectively.

III. RESULTS

The suggestion that nitrogen vacancies are responsible for the Raman activity in the LnN motivated careful measurements on films with widely differing V_N's for which the GdN results are displayed in Fig. 1. The conductivity in these films varies over four orders of magnitude, although all are relatively low implying no more than a few percent of nitrogen vacancies even in the most conductive film [2,26]. It is remarkable that there is no clear change in the spectra other than a weak 30% reduction from the least to the most conductive film. Both that change and a reduced strength of the sapphire substrate signal at 415 cm^{-1} result from a weakly increasing optical absorption in the LnN at the 2.43-eV excitation energy [23,27]. A similar set of experiments on V_N-doped LuN yield very similar results. There is clearly no sensitivity at all to the nitrogen-vacancy defects that dope the films; any disorder-activated features, thus, rely on other defects. Interestingly we also find a lack of clear dependence on the substrate; indeed even epitaxial (001) films grown on $LaAlO_3$ show the same spectra, with modest intensity differences between polarized and depolarized spectra.

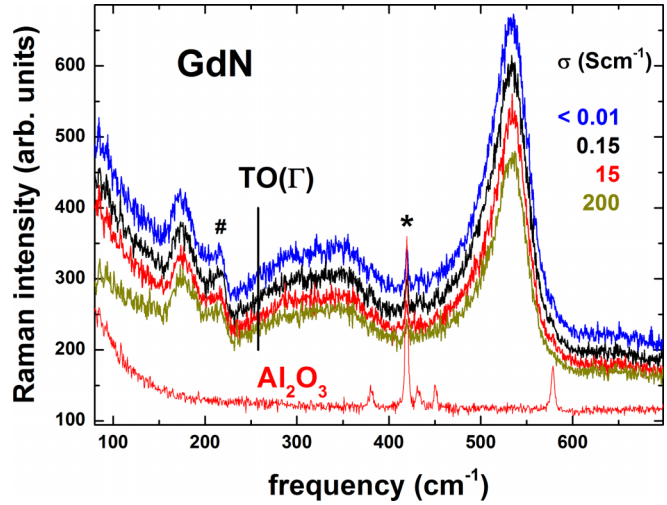

FIG. 1. Raman signals from GdN grown in ionized nitrogen at differing substrate temperatures. The entire signal falls weakly as the DC conductivity (see the legend) rises over more than four orders of magnitude. The lowest red curve was collected from a bare sapphire substrate, and its strongest line is seen with attenuated intensity in all of the GdN film spectra. The peak marked by a hash is not found in films grown with pure molecular N_2; it is a feature of an ion-generated defect so is disregarded when interpreting these data.

Before proceeding to a detailed discussion of the spectral weight in Fig. 1 it is useful to present next in Fig. 2, the computed dispersion curves for LuN and GdN from DFT modeling. The LuN dispersion is very similar to an earlier treatment [28] but shows significantly more dispersive branches than a previously published phonon computation for GdN [29]. We note that the previous GdN computation also showed no LO-TO splitting, in disagreement with the existence of TO(Γ) absorption in GdN [4]. In both materials, the phonons separate clearly into the lower-frequency acoustic band and higher-frequency optic branches. Along the high-symmetry lines, i.e., Γ-X and Γ-L, the acoustic branches show doubly degenerate TA and nondegenerate LA bands. The TA degeneracy is lifted along X-W and W-Γ.

The first point of experimental contact with the dispersion relates to infrared absorption data that unambiguously cite the TO(Γ) frequencies at 250 and 272 cm^{-1} in GdN and LuN, respectively [4], frequencies that are shown by the red symbols at Γ. The hollow blue symbols at the L point signal what was interpreted as LO(L) frequencies as determined by the assignment of the strong Raman feature in the 500–600-cm^{-1} range [6]. As discussed below, the current data suggest strongly that this feature is in fact LO(Γ) scattering mediated by the Fröhlich interaction, which is indicated by solid blue dots in Fig. 2. The agreement with the computed frequencies is decreased by the LO(Γ) assignment compared to the LO(L) assignment, although this disagreement remains less than 10%.

Returning now to the data, the spectra in Fig. 3 are compared there with the density of modes generated by the dispersion curves of Fig. 2. For comparison with the data, the van Hove singularities have been depressed by modest broadening. The DOM weight separates clearly into acoustic

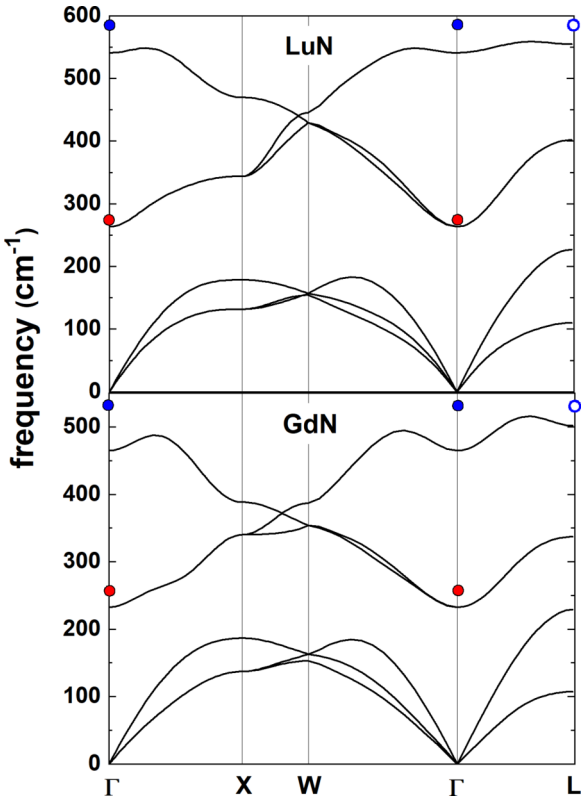

FIG. 2. The computed phonon dispersion curves for LuN (upper panel) and GdN (lower panel) along various lines within the Brillouin zone. The red dots represent measured frequencies from infrared absorption for the TO(Γ) at the zone center. The blue points represent the strong Raman feature found in the 500–600-cm^{-1} range for LnN with its previous assignment at the *L* point (hollow dots) and our new assignment of this feature near Γ (solid blue dots).

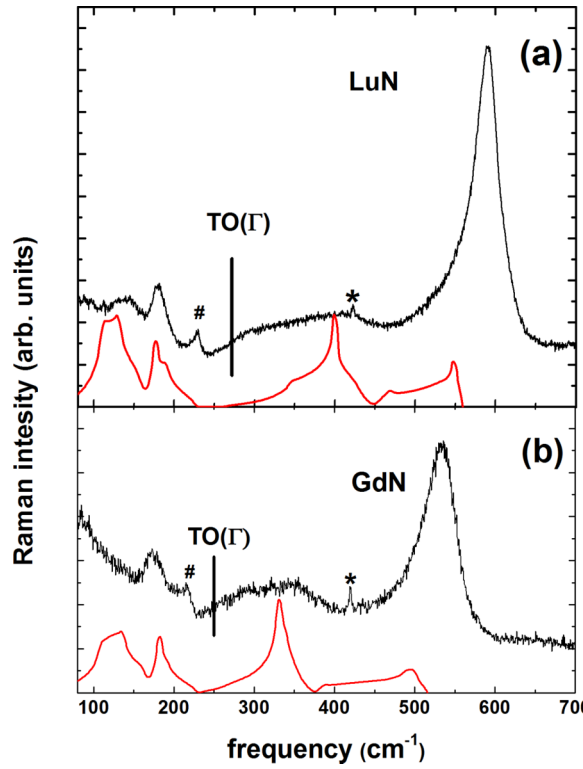

FIG. 3. Raman spectra of (a) LuN and (b) GdN compared directly with the density of modes derived from the phonon dispersions in Fig. 2. The starred peaks seen in GdN and less clearly in LuN derive from the sapphire substrate and the peak marked with a hash is associated with the unidentified defect found only in films grown with activated nitrogen. The spectra are similar, although shifted to a higher frequency in the reduced lattice constant of LuN. In addition to the strong LO(Γ), there are broad features below 700 cm^{-1} discussed in more detail in the text.

and optic branches. An asterisk labels the sapphire-substrate line mentioned above, and the feature marked by a hash is an unidentified line seen in these ion-grown films but absent from films grown in molecular N_2. Otherwise, the spectra follow the DOM bands with the exception of the very strong peak at 500–600 cm^{-1}. That feature occurs near the extreme highest frequency within the DOM. Its strength is severely anomalous, an issue that we discuss below after dealing with the more general broad DOM signal.

The influence of defect-activated scattering is especially interesting and informative in a comparison between films grown in ionized vs neutral molecular nitrogen shown in Fig. 4. One immediately notes that the band corresponding to the acoustic- and optic-branch DOMs are substantially stronger in the ion-grown film; doubtless the ions introduce excess defects. At the same time, there is a step in the scattering intensity across 250–300 cm^{-1} that shows no sensitivity to those defects. Its steplike pattern is reminiscent of two-phonon scattering in defect-free crystalline materials [30,31], which suggests the possibility of separating the two-phonon DOM. Thus in the inset we plot the difference [I(ion-assisted)-I (molecular N_2)], which remarkably follows the one-phonon DOM almost slavishly. The primary clear difference in that comparison is that the lowest-frequency band, arising from the TA branch and relating especially to TA(*X*) to TA(*W*) (see

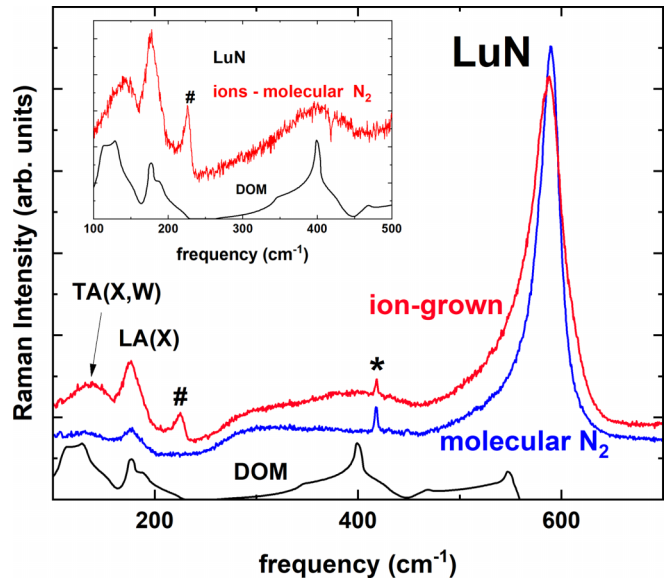

FIG. 4. Raman spectra of LuN grown in pure N_2 (blue) compared with a film grown in ionized nitrogen (red) in which the hash feature is an artifact as discussed in the text. The black curve is the computed DOM. The inset shows that the difference between the two curves shows remarkable agreement with the DOM.

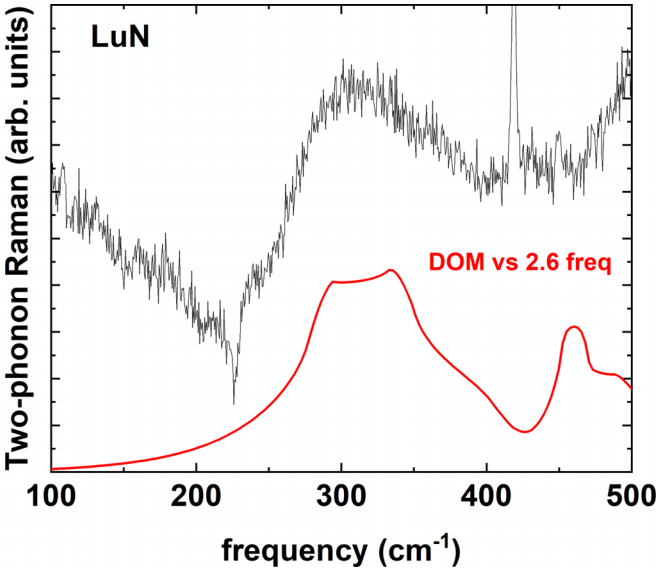

FIG. 5. The molecular-N_2-grown Raman spectrum of Fig. 4 with the defect-activated one-phonon DOM signal removed as described in the text. The red continuous line is the two-phonon TA DOM with the frequency adjusted up by 30% to illustrate an excellent agreement with the steplike rise across 250–300 cm^{-1}.

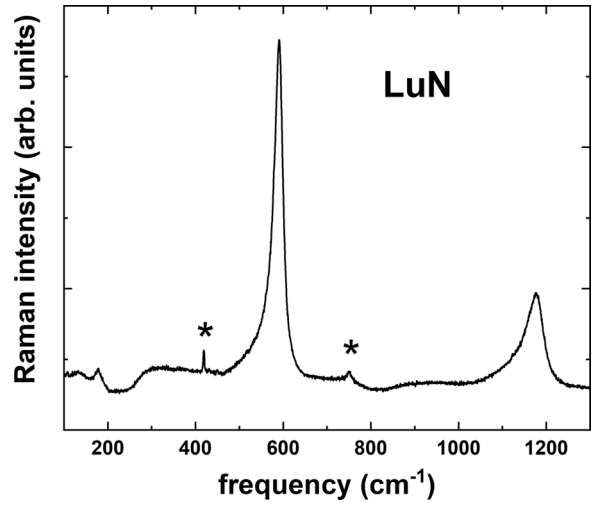

FIG. 6. Raman spectrum for molecular-N_2-grown LuN exhibiting strong first-order LO(Γ) scattering and its second-order peak at twice the frequency.

Fig. 2) is measured to be at somewhat higher frequency than the computed DOM. In contrast, the second acoustic peak relating to LA(X) appears as calculated.

Two-phonon Raman scattering in defect-free crystals arises from the combination of phonons with wave vectors summing to zero; the two phonons must have equal but opposite wave vectors [31]. The two-phonon DOM pattern is then a complex function involving the full set of TA, LA, TO, and LO branches in all combinations. However, the lowest-frequency onset necessarily arises from two phonons in the lowest-frequency acoustic branches so that the rapid rise seen here signals the two-phonon DOM in the TA branch. The wave-vector constraint, then, suggests a comparison with the one-phonon DOM plotted now vs double the frequency.

It is notable that the molecular-grown spectrum in Fig. 4 shows residual presence of the LA(X) line at ∼180 cm^{-1}. Thus, going one step further we have subtracted 35% of the defect signal in the inset of Fig. 4 from the molecular-grown signal in Fig. 4 to remove the peak and ultimately represent the two-phonon signal on its own. The result is compared with the sum of (2 TA + 2 LA) DOM spectrum in Fig. 5, with the computed phonon frequency increased by 30% as suggested above for the TA branch. The agreement is excellent, especially in view of the omission in the two-phonon DOM of TA+LA, TA+TO, and LA+TO components, which fill in the spectrum above 350 cm^{-1}. Thus, in both the defect-activated single-phonon DOM and the two-phonon signal, the computed dispersion appears to underestimate the TA phonon frequency by ∼30%.

We turn now to the prominent feature at 585 cm^{-1}, which has been assigned to LO(L) in previous studies of a range of LnN [6,7,10]. Initial reports suggested this mode is rendered Raman active by defects, most probably nitrogen vacancies [6], although subsequent measurements found no clear dependence on V_N [10]. Indeed Fig. 4 shows this peak as essentially unaffected by any defects present in these films; similar to the sapphire line at 415 cm^{-1}, it is marginally stronger in the more transparent molecular-nitrogen-grown film and does not follow the defect dependency of the density-of-modes signal. That lack of dependence on V_N is seen also in the GdN data in Fig. 1. The scattering appears to be independent of defect concentration; it appears intrinsic rather than defect activated.

In view of the apparently intrinsic nature of the prominent feature it is necessary to ask how the wave vector and symmetry selection rules are accommodated. It is important to note that the model proposed for the Raman-scattering strength of the LO(L) scattering in Eu monochalcogenides suggests the feature as a one phonon-one spin excitation [9,32], an assignment that is clearly unavailable in LuN's zero spin state. In light of this, we propose this feature to be forbidden LO(Γ) scattering induced by the Fröhlich interaction as seen in YbS [12]. Within this model excitons interact with the macroscopic electric field produced by the LO phonons via the Fröhlich interaction [31,33]. This exciton-phonon coupling activates scattering near Γ, and when near resonance, can produce very strong scattering and multiphonon scattering [12,31]. Similar to YbS, the LnN exhibit strong intrinsic LO(Γ) Raman scattering and evidence of multiphonon features [12]. Figure 6 shows a peak in LuN at twice the frequency of the first-order peak, which we also observe in GdN.

One notes that the assignment of the strong LO Raman signal as arising from LO(Γ) rather than LO(L) increases the disagreement for the DFT calculation especially for GdN. The disagreement is, however, still less than 10%, considerably less than found above for the TA branch. The application of the DFT-based techniques to the $4f$ materials remains poorly developed, so such disagreements are not unexpected. It is notable that DFT-based computations lead variously to metallic and both direct- and indirect-gap predictions for the LnN [24,34–37].

IV. CONCLUSIONS

We have performed Raman-scattering spectroscopy on a series of GdN and LuN films with a wide range of nitrogen vacancies (V_N) and, thus, carrier concentrations. The primary target of the investigation was clarification of the Raman activity of the most prominent feature, previously suggested as a defect-activated Raman signal from the LO(L) vibration, speculated as being activated by nitrogen vacancies. The results show no dependence at all on V_N, or indeed on any other structural difference among the films. A suggestion of scattering by magnetic disorder, a one-phonon one-magnon (or one-spin above the Curie temperature) event can be discarded by the strength of the feature in nonmagnetic LuN. The full set of results suggests strongly that the signal arises from the LO(Γ) mode mediated by the Fröhlich interaction.

Spectra were collected across 100–700 cm^{-1} and compared with the one-phonon DOM computed within a DFT treatment. The weaker features within the 100–700-cm^{-1} range *do* show dependence on defects, although not specifically with V_N. The spectrum associated with those followed very closely the one-phonon DOM, exactly as expected for point defects. The only disagreement occurs in the lowest TA branch DOM, which appears at higher frequency in the measured as compared to the computed TA branch.

In the spectra of films with reduced defect concentration, there remained a signal rising sharply between 200 and 300 cm^{-1} signaling two-phonon scattering events. That rise suggested that the computed TA-branch frequencies are systematically ∼30% low, which as mentioned above can also be seen in the defect-activated one-phonon Raman spectrum.

The data point to a need for improving the calculated phonon dispersion in these materials. The calculation returns a ∼30% underestimate of the TA-branch frequency and a smaller but non-negligible underestimate for the LO(Γ) frequency.

ACKNOWLEDGMENTS

This research was supported by the New Zealand Endeavour Fund (Grant No. RTVU1810). The computations were performed on the Räpoi high performance computing facility of Victoria University of Wellington. The MacDiarmid Institute was supported under the New Zealand Centres of Research Excellence Programme. We have benefited from numerous conversations with R. G. Buckley. We are indebted to an unnamed referee for bringing Ref. [12] to our attention.

[1] F. Hulliger, Magnetic properties of the rare earth pnictides, J. Magn. Magn. Mater. **8**, 183 (1978).

[2] F. Natali, B. J. Ruck, N. O. Plank, H. J. Trodahl, S. Granville, C. Meyer, and W. R. Lambrecht, Rare-earth mononitrides, Prog. Mater. Sci. **58**, 1316 (2013).

[3] S. Nishio, T. Nakagawa, T. Arakawa, N. Tomioka, T. A. Yamamoto, T. Kusunose, K. Niihara, T. Numazawa, and K. Kamiya, Specific heat and thermal conductivity of HoN and ErN at cryogenic temperatures, J. Appl. Phys. **99**, 08K901 (2006).

[4] W. F. Holmes-Hewett, R. G. Buckley, T. J. Butler, C. Pot, K. Van Koughnet, B. J. Ruck, and H. J. Trodahl, TO(Γ) mode resonances in the rare-earth nitrides, AIP Adv. **12**, 075120 (2022).

[5] L. Degiorgi, S. Teraoka, G. Compagnini, and P. Wachter, Optical and Raman investigation of Yb pnictide compounds, Phys. Rev. B **47**, 5715 (1993).

[6] S. Granville, C. Meyer, A. R. H. Preston, B. M. Ludbrook, B. J. Ruck, H. J. Trodahl, T. R. Paudel, and W. R. L. Lambrecht, Vibrational properties of rare-earth nitrides: Raman spectra and theory, Phys. Rev. B **79**, 054301 (2009).

[7] K. Upadhya, R. Kumar, Q. Li, B. Sun, and B. Saha, Vibrational spectrum and thermal conductivity of rare-earth semiconducting erbium nitride thin films, Phys. Status Solidi RRL, **16** 2200029 (2022).

[8] J. C. Tsang, M. S. Dresselhaus, R. L. Aggarwal, and T. B. Reed, Inelastic light scattering in the europium chalcogenides, Phys. Rev. B **9**, 984 (1974).

[9] G. Güntherodt, R. Merlin, and P. Grünberg, Spin-disorder-induced Raman scattering from phonons in europium chalcogenides. i. experiment, Phys. Rev. B **20**, 2834 (1979).

[10] A. Shaib, F. Natali, J. R. Chan, F. Ullstad, W. F. Holmes-Hewett, J. D. Miller, B. J. Ruck, and H. J. Trodahl, Coexisting structural phases in the catalytically driven growth of rock salt GdN, Mater. Res. Express **7**, 046404 (2020).

[11] G. Travaglini, F. Marabelli, R. Monnier, E. Kaldis, and P. Wachter, Electronic structure of ScN, Phys. Rev. B **34**, 3876 (1986).

[12] R. Merlin, G. Güntherodt, R. Humphreys, M. Cardona, R. Suryanarayanan, and F. Holtzberg, Multiphonon processes in YbS, Phys. Rev. B **17**, 4951 (1978).

[13] T. R. Paudel and W. R. L. Lambrecht, Calculated phonon band structure and density of states and interpretation of the Raman spectrum in rocksalt ScN, Phys. Rev. B **79**, 085205 (2009).

[14] F. Ullstad, G. Bioletti, J. R. Chan, A. Proust, C. Bodin, B. J. Ruck, J. Trodahl, and F. Natali, Breaking molecular nitrogen under mild conditions with an atomically clean lanthanide surface, ACS Omega **4**, 5950 (2019).

[15] J. R. Chan, S. G. Lambie, H. J. Trodahl, D. Lefebvre, M. Le Ster, A. Shaib, F. Ullstad, S. A. Brown, B. J. Ruck, A. L. Garden, and F. Natali, Facile dissociation of molecular nitrogen using lanthanide surfaces: Towards ambient temperature ammonia synthesis, Phys. Rev. Mater. **4**, 115003 (2020).

[16] P. Giannozzi, S. Baroni, N. Bonini, M. Calandra, R. Car, C. Cavazzoni, D. Ceresoli, G. L. Chiarotti, M. Cococcioni, I. Dabo, A. D. Corso, S. de Gironcoli, S. Fabris, G. Fratesi, R. Gebauer, U. Gerstmann, C. Gougoussis, A. Kokalj, M. Lazzeri, L. Martin-Samos *et al.*, QUANTUM ESPRESSO: A modular and open-source software project for quantum simulations of materials, J. Phys.: Condens. Matter **21**, 395502 (2009).

[17] A. Floris, S. de Gironcoli, E. K. U. Gross, and M. Cococcioni, Vibrational properties of MnO and NiO from DFT $+u$-based density functional perturbation theory, Phys. Rev. B **84**, 161102(R) (2011).

[18] P. Giannozzi Jr, O. Andreussi, T. Brumme, O. Bunau, M. B. Nardelli, M. Calandra, R. Car, C. Cavazzoni, D. Ceresoli, M. Cococcioni, N. Colonna, I. Carnimeo, A. D. Corso, S. de Gironcoli, P. Delugas, R. A. DiStasio, A. Ferretti, A. Floris, G. Fratesi, G. Fugallo *et al.*, Advanced capabilities for materials modelling with quantum ESPRESSO, J. Phys.: Condens. Matter **29**, 465901 (2017).

[19] P. Giannozzi, O. Baseggio, P. Bonfà, D. Brunato, R. Car, I. Carnimeo, C. Cavazzoni, S. de Gironcoli, P. Delugas, F. Ferrari Ruffino, A. Ferretti, N. Marzari, I. Timrov, A. Urru, and S. Baroni, Quantum espresso toward the exascale, J. Chem. Phys. **152**, 154105 (2020).

[20] A. Floris, I. Timrov, B. Himmetoglu, N. Marzari, S. de Gironcoli, and M. Cococcioni, Hubbard-corrected density functional perturbation theory with ultrasoft pseudopotentials, Phys. Rev. B **101**, 064305 (2020).

[21] M. Topsakal and R. Wentzcovitch, Accurate projected augmented wave (PAW) datasets for rare-earth elements (RE=La-Lu), Comput. Mater. Sci. **95**, 263 (2014).

[22] H. J. Trodahl, A. R. H. Preston, J. Zhong, B. J. Ruck, N. M. Strickland, C. Mitra, and W. R. L. Lambrecht, Ferromagnetic redshift of the optical gap in GdN, Phys. Rev. B **76**, 085211 (2007).

[23] S. Devese, K. Van Koughnet, R. G. Buckley, F. Natali, P. P. Murmu, E.-M. Anton, B. J. Ruck, and W. F. Holmes-Hewett, Probing the defect states of $LuN_{1-\delta}$: An experimental and computational study, AIP Adv. **12**, 035108 (2022).

[24] P. Larson, W. R. L. Lambrecht, A. Chantis, and M. van Schilfgaarde, Electronic structure of rare-earth nitrides using the LSDA+U approach: importance of allowing $4f$ orbitals to break the cubic crystal symmetry, Phys. Rev. B **75**, 045114 (2007).

[25] W. F. Holmes-Hewett, Electronic structure of nitrogen-vacancy doped SmN: Intermediate valence and $4f$ transport in a ferromagnetic semiconductor, Phys. Rev. B **104**, 075124 (2021).

[26] S. Granville, B. J. Ruck, F. Budde, A. Koo, D. J. Pringle, F. Kuchler, A. R. H. Preston, D. H. Housden, N. Lund, A. Bittar, G. V. M. Williams, and H. J. Trodahl, Semiconducting ground state of GdN thin films, Phys. Rev. B **73**, 235335 (2006).

[27] W. F. Holmes-Hewett, C. Pot, R. G. Buckley, A. Koo, B. J. Ruck, F. Natali, A. Shaib, J. D. Miller, and H. J. Trodahl, Nitrogen vacancies and carrier-concentration control in rare-earth nitrides, Appl. Phys. Lett. **117**, 222409 (2020).

[28] C. Li and D. Broido, Phonon thermal transport in transition-metal and rare-earth nitride semiconductors from first principles, Phys. Rev. B **95**, 205203 (2017).

[29] V. Mankad, S. K. Gupta, and P. K. Jha, Ab initio investigation on structural, electronic and lattice dynamical properties of MgN and GdN crystals, Results Phys. **2**, 34 (2012).

[30] B. Weinstein and M. Cardona, Two-phonon Raman spectra of Si and GaP, Solid State Commun. **10**, 961 (1972).

[31] M. Cardona, Resonance phenomena, in *Light Scattering in Solids II: Basic Concepts and Instrumentation*, edited by M. Cardona and G. Güntherodt (Springer, Berlin/Heidelberg, 1982), pp. 19–178.

[32] R. Merlin, R. Zeyher, and G. Güntherodt, Spin-Disorder-Induced Raman Scattering in Europium Chalcogenides, Phys. Rev. Lett. **39**, 1215 (1977).

[33] Y. Toyozawa and J. Hermanson, Exciton-Phonon Bound State: A New Quasiparticle, Phys. Rev. Lett. **21**, 1637 (1968).

[34] A. Galler and L. Pourovskii, Electronic structure of rare-earth mononitrides: quasiatomic excitations and semiconducting bands, New J. Phys. **24**, 043039 (2022).

[35] C. M. Aerts, P. Strange, M. Horne, W. M. Temmerman, Z. Szotek, and A. Svane, Half-metallic to insulating behavior of rare-earth nitrides, Phys. Rev. B **69**, 045115 (2004).

[36] C.-G. Duan, R. F. Sabiryanov, J. Liu, W. N. Mei, P. A. Dowben, and J. R. Hardy, Strain Induced Half-Metal to Semiconductor Transition in GdN, Phys. Rev. Lett. **94**, 237201 (2005).

[37] C.-G. Duan, R. F. Sabirianov, W.-N. Mei, P. A. Dowben, S. Jaswal, and E. Y. Tsymbal, Electronic, magnetic and transport properties of rare-earth monopnictides, J. Phys.: Condens. Matter **19**, 315220 (2007).